Morphological and Elemental Classification of Freshly Emitted Soot Particles and Atmospheric Ultrafine Particles using the TEM/EDS

Laarnie Tumolva,[1] Ji-Yeon Park,[1] Jae-suk Kim,[1] Arthur L. Miller,[2] Judith C. Chow,[3] John G. Watson,[3] and Kihong Park[1]

[1]*Research Center for Biomolecular Nanotechnology, Department of Environmental Science and Engineering, Gwangju Institute of Science and Technology, Gwangju, Korea*
[2]*National Institute for Occupational Safety and Health, Spokane, Washington, USA*
[3]*Desert Research Institute, Reno, Nevada, USA*

The Transmission Electron Microscopy (TEM) and Energy Dispersive Spectroscopy (EDS) were used to determine morphology and elemental composition of a variety of freshly emitted soot particles (acetylene flame, candle flame, kerosene flame, diesel exhaust, electric arc, plastic burning, styrofoam burning, wood burning [white oak and pine bark], and rice straw burning), which can be possible candidate soot in the ambient atmosphere, and ultrafine particles sampled in urban, industrial, and coastal sites during ultrafine particle formation events (combustion and photochemical events). By using mobility-classified non-refractory ((NH$_4$)$_2$SO$_4$) and refractory (Polystyrene latex (PSL) and salt (NaCl)) particles, limitation of the TEM was tested. Data showed that the TEM method can be used to examine shapes of both volatile particles such as (NH$_4$)$_2$SO$_4$ (100 nm) at low, but not high magnification (refer to low and high beam intensity, respectively), and nonvolatile particles like NaCl (100 nm) and PSL (84 nm) at either low or high magnification. Distinct differences in morphological properties such as primary particle diameter, fractal dimension, and microstructure were observed among the different types of fresh soot particles. The atmospheric ultrafine particles were classified as agglomerates, sulfate mixtures (spherical), metallic oxides (spherical and polygonal), C-rich refractory (not agglomerated), C-rich non-refractory (not agglomerated), Si-rich (spherical), Na-rich (porous), or P-containing (non-spherical) particles. At the urban Gwangju site, a higher fraction of fresh and aged agglomerates was observed than at other sites. The C-rich non-refractory and sulfate mixtures were often observed in the photochemical event. The C-rich refractory particles were abundant at the Gwangju and Yeosu sites. The coastal Taean site had few agglomerates due to limited anthropogenic combustion source.

INTRODUCTION

Fine and ultrafine particles in the ambient atmosphere are of current interest due to their potential impact on human health, radiation balance, cloud formation, visibility impairment, and atmospheric chemistry. In particular, ultrafine particles (<100 nm) may have especially high levels of toxicity and reactivity due to their elevated surface-area-to-volume ratio (Peters et al. 1997; Oberdörster 2000). A high concentration of ultrafine particles may also lead to an increase in alveolar deposition, as has been reported in animal studies and in vitro cell studies (Oberdörster et al. 2005). It has been shown that the morphological properties of atmospheric particles play an important role in their transport behavior, deposition patterns in the human respiratory system (Oberdörster 2001) and interactions in the human lung (Stearns et al. 2001). Optical properties of irregular particles may significantly differ from a compact sphere (Bond and Bergstrom 2006).

Atmospheric ultrafine particles are either emitted directly from a wide range of sources or formed by gas-to-particle conversion processes. The major types of ultrafine particles in the ambient atmosphere include sulfates, nitrates, and ammonium (Friedlander 2000) and carbonaceous particles which are comprised of both organic and elemental carbon (OC and EC), and the OC can dominate the bulk mass of soot (50–90%) (Katrinak et al. 1992), depending on the type of sources and processes (Szidat et al. 2007; Grieshop et al. 2009). Soot particles are defined here as carbonaceous particles having an irregular agglomerate structure consisting of spherical primary particles (Xiong and Friedlander 2001; Park et al. 2003; Wentzel et al. 2003; Hu and Koylu 2004; Jung et al. 2004; Park et al. 2004; Kocbach et al. 2006). They originated from a variety of anthropogenic combustion sources and biomass burning (Friedlander 2000; Xiong and Friedlander 2001). The morphology of particles has been found to differ among sources and combustion conditions. For example, vehicle exhaust particles (i.e., typically produced from high temperature combustion process)

are usually highly agglomerated having a high surface-area-to-mass ratio (Kocbach et al. 2006). The morphologies of ultrafine particles on and near a freeway were found to be aggregate, electron-opaque sphere, electron-transparent sphere, irregularly shaped particles, and particles with multiple inclusions (Barone and Zhu 2008). Polymer burnings, such as plastic bags and styrofoam, usually occurring in waste incinerators, can produce soot particles with highly toxic substances (e.g., dioxin). Burning biomass fuels (e.g., woods, agricultural residues, etc.) through a variety of different combustion processes (e.g., flaming and smoldering) can emit a range of carbonaceous particles (Posfai et al. 2003). Particles from biomass burning can also contain toxins due to the inclusion of cellulose, hemicellulose, and lignin in the biomass fuel (McKenzie et al. 1995). Due to the high surface-area-to-mass ratio of the agglomerated soot particles, they may have high ability of reactivity, and provide condensational sink for toxic vapor compound such as dioxin. Most previous studies have focused on morphological properties of specific soot particles from flame and diesel engines (Dobbins 2007), vehicle exhaust and residential wood smoke (Kocbach et al. 2006), diesel and Palas (Wentzel et al. 2003), or biomass burning (Posfai et al. 2003) rather than comparing morphological properties among a variety of soot particles. In addition to those soot particles, spherical or non-spherical sulfates, organics, metals, and so on can constitute the atmospheric ultrafine particles in an urban area (Friedlander 2000). Although there have been a lot of studies on morphological and elemental properties of ultrafine particles (Maynard 2000), there has been limited database on the properties of atmospheric ultrafine particles during ultrafine particle formation events (photochemical and combustion event).

In this study, limitation of the Transmission Electron Microscopy (TEM) (i.e., high vacuum condition and high electron beam intensity) was first tested by using mobility-classified non-refractory (e.g., ammonium sulfate (($NH_4)_2SO_4$)) and refractory (Polystyrene latex (PSL) and sodium chloride (NaCl)) particles. Morphology and elemental composition of a variety of freshly emitted carbonaceous soot particles from acetylene flame, candle flame, kerosene flame, diesel exhaust, electric arc, plastic burning, styrofoam burning, wood (white oak and pine bark) burning, and rice straw burning, which can be possible candidate soot in the ambient atmosphere, were then examined. Atmospheric ultrafine particles were classified into several distinct types according to their morphology and elemental composition sampled in urban, industrial, and coastal sites during ultrafine particle formation events (photochemical and combustion events). Additionally, the number of each type of particles at the different sites was determined.

EXPERIMENTAL

Figure 1 provides a schematic outline of the current experimental setup. Atmospheric ultrafine particles were sampled at
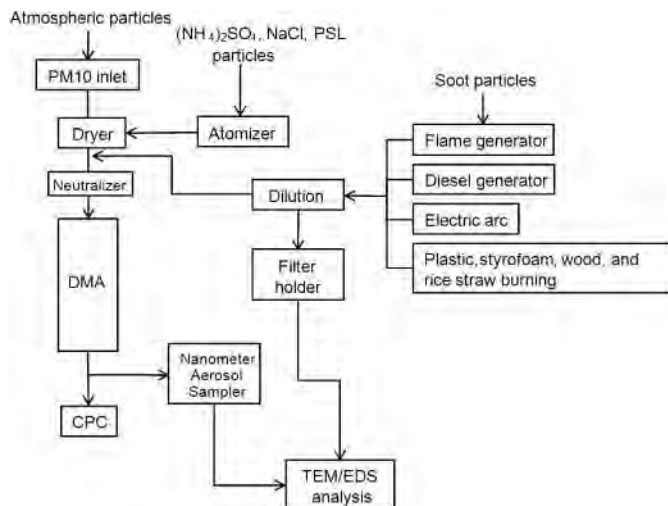

FIG. 1. A schematic outline of the experimental setup (DMA: Differential Mobility Analyzer, CPC: Condensation Particle Counter, TEM: Transmission Electron Microscopy, EDS: Energy Dispersive Spectroscopy).

three different sites (Gwangju, Yeosu, and Taean in Korea). Detailed description on the sampling sites was given in our previous paper (Park et al. 2008). Gwangju is an urban site surrounded by multiple pollution, including agricultural, traffic, industrial, and residential activities. Yeosu is an industrial site, located in a coastal area where petrochemical and steel manufacturing industries are present, and Taean is a coastal and continental background site. The atmospheric particles were drawn through a PM_{10} inlet, dried out by a dryer (Nafion MD-110, USA), and introduced into either the Differential Mobility Analyzer (DMA) or the Scanning Mobility Particle Sizer (SMPS). The SMPS consisted of a DMA (TSI 3081, USA) and a condensation particle counter (CPC) (TSI 3022A, USA). The size distribution of the ambient aerosols was monitored continuously to determine the peak mode diameter of ultrafine particles (<100 nm) with the highest concentration. When enhanced ultrafine particle concentration was observed (i.e., ultrafine particle event), the particles with an ultrafine mode diameter were selected by the DMA and collected on a TEM grid using either a nano-aerosol sampler (TSI 3089, USA) or a filter sampler.

For the laboratory-generated aerosols tests, $(NH_4)_2SO_4$ (Sigma Aldrich, USA) polystyrene latex (PSL)(84 ± 9 nm, Duke Scientific, USA), and NaCl (Sigma Aldrich, USA) particles were produced using a Collision atomizer (TSI 3076, USA). The water solution was continuously aerosolized into droplets through compressed air in the atomizer. Droplets containing any suspended particles or dissolved solids were dried out by a series of two diffusion driers. The liquid droplets containing suspended particles were evaporated through driers (i.e., water solvent was evaporated), enabling only the particles to be suspended in the air. Any dissolved solids in the droplets were crystallized during the drying process into particle phases

TABLE 1
Summary of all particles tested

Particle type	Mobility size, nm	Source or generation method
Atmospheric submicron particles	[a]20 nm, 25 nm, 30 nm, 35 nm, 40 nm, 50 nm, 70 nm, 80 nm, 90 nm, 100 nm, 130 nm, 160 nm	Urban Gwangju, Korea, industrial Yeosu, Korea, coastal Taean, Korea
Ammonium sulfate particles	[a]100 nm	Atomization
PSL particles	[a]84 nm	Atomization
Sodium chloride particles	[a]100 nm	Atomization
Acetylene flame soot	[b]5 nm ∼ 50 nm	Flame
Candle flame soot	[b]10 nm ∼ 100 nm	Flame
Kerosene flame soot	[b]20 nm ∼ 600 nm	Flame
Diesel exhaust soot	[b]20 nm ∼ 300 nm	Diesel generator
Electric arc soot	[b]20 nm ∼ 300 nm	Palas electric arc
Plastic burning soot	[b]10 nm ∼ 200 nm	Plastic bag
Styrofoam burning soot	[b]10 nm ∼ 200 nm	Styrofoam
Wood burning soot	[b]30 nm ∼ 300 nm	White oak
Wood burning soot	[b]30 nm ∼ 100 nm, [c]200 nm ∼ 10 um	Pine bark
Rice straw burning soot	[b]30 nm ∼ 600 nm	Rice straw

[a]mobility size selected by the DMA.
[b]particle size range measured by the SMPS.
[c]particle size range measured by the PSD Analyzer.

in the air. A DMA was used to select particles of a specified mobility size.

As summarized in Table 1, the fresh soot particles were produced from an acetylene flame, a candle flame, a kerosene flame, diesel exhaust, an electric arc, plastic burning, styrofoam burning, wood burning (white oak and pine bark), and rice straw burning. A 2 inch flame acetylene torch was used to produce acetylene flame soot particles that were sampled on a TEM grid at a dilution ratio of 17 and sampling time of 20 min. For the generations of candle and kerosene flame soot particles, a 10 inch shroud was used as a housing to prevent outside air from disturbing the flame. The generated soot particles were extracted through a 6 mm hole of the glass sampling probe with an internal diameter of 10 mm and diluted with 20 liter per minute (lpm) of clean dry air. Particles were collected at a flow rate of 1 lpm on a TEM grid which was taped on a filter holder. The height of flame for each fuel used was noted. To generate the diesel soot particles, particles were sampled from a diesel generator (Onan-Cummins powered by a three cylinder, 1.5 liter Isuzu engine) operated at 4 kW and diluted with filtered air at a flow rate of 5 lpm and subsequently collected on a TEM grid using a filter sampler for a period of 40 min. A Palas electric arc (GfG 1000, USA) operated at 950 a.u. current was used to produce electric arc soot particles, which were subsequently diluted with air at a dilution ratio of 8 and collected on a TEM grid for a sampling duration of 40 min. A plastic bag and styrofoam burned in an aluminum can to produce soot. A stove was used to burn wood and rice straw and the soot was collected. For the wood combustion particles, white oak was used to produce particles in the

flame phase, while pine bark was used to produce particles in the smoldering phase. Both were sampled on a TEM grid at a dilution ratio of 40 and a sampling duration of 25 min. The dried rice straw, a common residue found in Korea after harvesting rice, was burned to produce the rice straw soot in both the flaming and smoldering phases. The combustion conditions were identified by measuring the exhaust temperature and CO/CO_2 ratio. To determine the size distribution of the soot particles, the SMPS was used.

The TEM grid used in the study was carbon film coated 200 mesh copper grid (Electron Microscopy Sciences, USA). Samples were stored in a polystyrene Petri dish and equilibrated in a desiccating chamber at a constant temperature ($\sim$25°C), and relative humidity ($\sim$20%) before imaging. Morphologies of individual particles using the TEM (JEOL JEM-2100, USA) and their elemental compositions were determined by Energy Dispersive Spectroscopy (EDS) (OXFORD INCAx–sight, USA). The TEM was operated at a 200 kV accelerating voltage and 102 μA beam current. By measuring the spectrum of blank areas between particles, the background signal of the TEM grid was corrected. Digital Micrograph 3 software (Gatan Inc., USA) was used for the TEM image analysis.

RESULTS AND DISCUSSION

Morphological and Elemental Classification of Laboratory-Generated Particles

To examine particle shape changes under a low vacuum condition and high electron beam intensity in the TEM, $(NH_4)_2SO_4$,
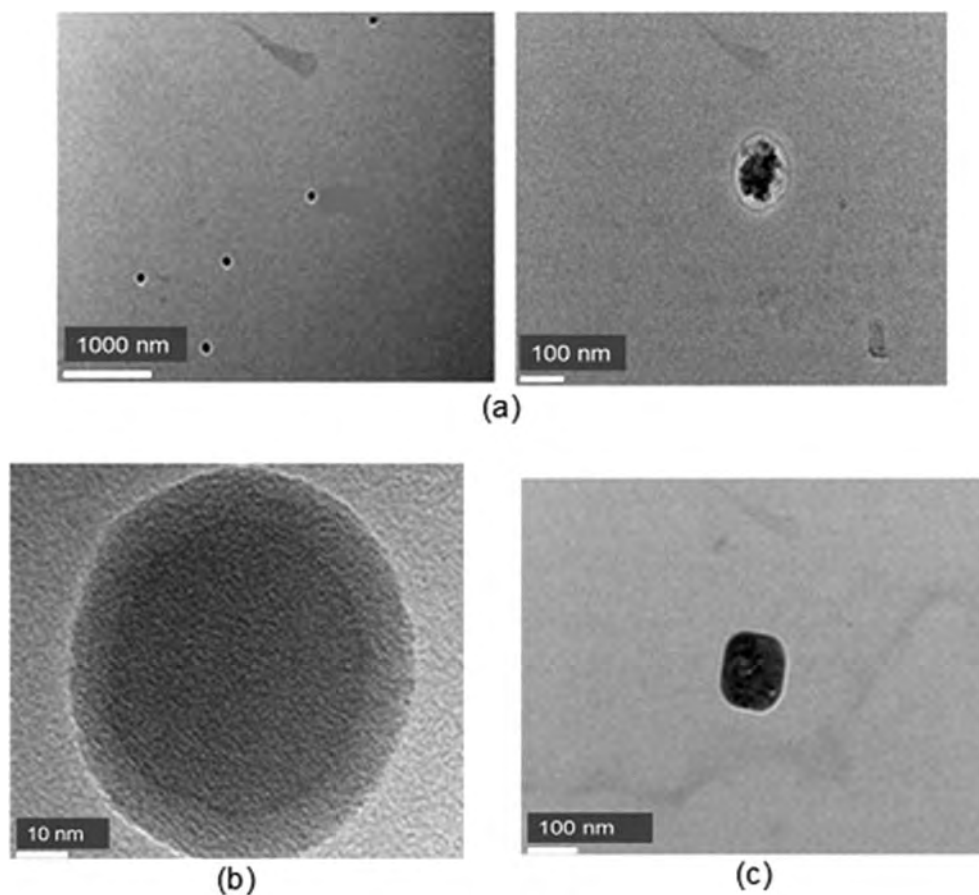
FIG. 2. TEM images of mobility-classified particles: (a) 100 nm ammonium sulfate ((NH_4)$_2$$SO_4$) under low (left) and high (right) magnification, (b) 84 nm Polystyrene latex (PSL) under high magnification, and (c) 100 nm sodium chloride (NaCl) particles under high magnification.

PSL, and NaCl particles were used. Figure 2 shows the TEM images of 100 nm mobility-classified (NH_4)$_2$$SO_4$ particles at both low (left) and high (right) magnification (i.e., low and high electron beam intensity, respectively). The (NH_4)$_2$$SO_4$ particles were spherical at low magnification, but had a residue with a beam-damaged outer area at high magnification, indicating that for non-refractory particles like (NH_4)$_2$$SO_4$, the original shape cannot be accurately determined at high magnification. On the other hand, NaCl and PSL showed no significant difference between low and high magnification. Their projected area equivalent sizes obtained from the TEM images were similar to the mobility size (100 nm) for NaCl and the specified size (84 nm) for PSL, also suggesting that the shape of such refractory particles remained unchanged.

To quantify the morphological properties of soot agglomerate that consists of spherical primary particles, the number and size of the primary particles, the fractal dimension, and the agglomerate size (e.g., length, width, projected area equivalent diameter) can be used. In this study, the soot particles are considered as having a chain-like agglomerated shape and a dominant element of C in its background-corrected EDS spectrum. Table 2 summarizes morphological and elemental properties of

the soot or carbonaceous particles tested in this study. Their corresponding TEM images are also shown in Figure 3. Distinct differences in the morphological properties among different types of soot particles were found. As shown in Table 2, the kerosene flame soot showed the highest mean primary particle diameter (33.9 ± 17.5 nm), while the acetylene flame soot exhibited the lowest (23.5 ± 7.4 nm). Precursor carbon radicals and kinetic factors may affect the size distribution of primary particles. The precursor carbon radicals undergo carbonization, forming polycyclic aromatic hydrocarbons (PAH), which is the precursor of soot (Pugmire et al. 2002). For example, the diesel exhaust soot and some of the flame soot, depending on the engine load and flame conditions, showed similar PAH composition and formation (Dobbins 2007), leading to a similar primary particle size. The kinetic factors to form precursor molecules may also affect primary particle size. The soot from burning styrofoam and plastic contained a significant amount of condensed species, as shown in Figures 3b and c, and their primary particles were indistinct.

The fractal dimension was determined by using the relationship between the primary particles and the number of primary particles calculated from the projected areas of agglomerates

TABLE 2

Summary of morphological and elemental properties of laboratory-generated soot or carbonaceous particles

Source	Primary particle diameter (nm)		Maximum length (nm)		Fractal dimension	Microstructure	Major elements	Minor elements
	Mean	Standard deviation	Mean	Standard deviation				
Acetylene flame	23.5	7.4	180	72	2.11	Ordered layers	C	O, Fe
Candle flame	26.3	6.2	135	42	2.16	Ordered layers	C	O, Si
Kerosene flame	33.9	17.5	1157	659	1.69	Ordered layers	C	O, Si
Diesel exhaust	24.0	3.5	262	222	1.69	Ordered layers	C	O
Electric arc	—[a]	—[a]	249	107	—[a]	Amorphous	C	O, Si
Plastic burning	—[b]	—[b]	527	320	—[b]	Amorphous	C	Si, O
Styrofoam burning	—[b]	—[b]	347	180	—[b]	Amorphous	C	O
White oak burning in the flaming phase	32.7	9.9	445	376	1.72	Ordered layers	C, K	Cl, O, S, Si
Pine bark burning in the smoldering phase	—[c]	—[c]	—[c]	—[c]	—[c]	Amorphous	C,	O, S
Rice straw burning in the flaming phase	29.2	5.1	143	90	1.84	Ordered layers	C, K	Cl, O, S, Si
Rice straw burning in the smoldering phase	—[c]	—[c]	—[c]	—[c]	—[c]	Amorphous	C, K	O, S, Si, Al

[a] not determined due to indistinct primary particles.
[b] not determined due to heavy coating.
[c] not agglomerated (spherical).

as well as the ratio of the maximum length to primary particle diameter (Park et al. 2004). The mean value of the maximum length of the agglomerate ranged from 135 ± 42 nm (candle flame soot) to 1157 ± 659 nm (kerosene flame soot). By considering the overlap of primary particles to calculate their number (Oh and Sorensen 1997), we obtained a higher number of primary particles in the agglomerate, resulting in a higher fractal dimension. With the exception of the soots from electric arc, plastic burning, and styrofoam burning, the number of primary particles in all types of agglomerates showed a linear dependence on the ratio of the maximum length to the primary particle diameter, suggesting that they are all fractal-like. The fractal dimension of the soots from electric arc, plastic burning, and styrofoam burning was not determined due to their indistinct primary particles.

As shown in Figure 3 and Table 2, the fractal dimension decreased as the agglomerate shape became more irregular and less compact. The candle flame and acetylene flame soot indicated the highest fractal dimensions (2.16 and 2.11, respectively), while kerosene flame and diesel soot had the lowest value (i.e., 1.69). In other words, the candle flame soot had the most compact structures, while the diesel exhaust and kerosene flame soot had the most branched structures among the different types of soot tested. Based on fractal dimension analysis, the soot can be categorized as an aggregation either formed by particle-cluster (fractal dimension >2), the primary particles diffuse to a cluster of primary particles, or cluster-cluster (fractal dimension <2), the clusters of primary particles attach to each other.

Data for the particle mobility size distribution (Table 1), measured with the SMPS, and length (Table 2), measured with the TEM, showed that agglomerates produced from the laminar flame (i.e., acetylene and candle flames) had a more uniform size compared to those produced from the turbulent flame (i.e., kerosene), diesel engine combustion, and wood burning which produced both large and small agglomerates. This might have occurred because soot precursors coexist with agglomerates in the turbulent processes (Hu and Koylu 2004). A laminar flame is characterized by the flame and smoke flowing in a uniform direction. In a turbulent flame, however, the flow of flame and smoke is chaotic. The kerosene flame generated very large agglomerates and the heavy soot and aggregate collisions in the dense smoke observed in this flame may have contributed to the presence of superaggregates (Kim et al. 2006).

In the smoldering phase of pine bark combustion, the ignited fuel charred and released smoke continuously, and particles were sampled directly from the smoke plume. Figure 4 shows TEM images of pine bark particles in the smoldering phase with a significant amount of spherical particles (i.e., tar ball, left figure). This is in contrast to particles from burning white oak in the flaming phase, as shown in Figure 3f. Mckenzie et al. (1995) reported that the pine bark burning had lower combustion efficiency, favoring the smoldering phase, and emitted a higher
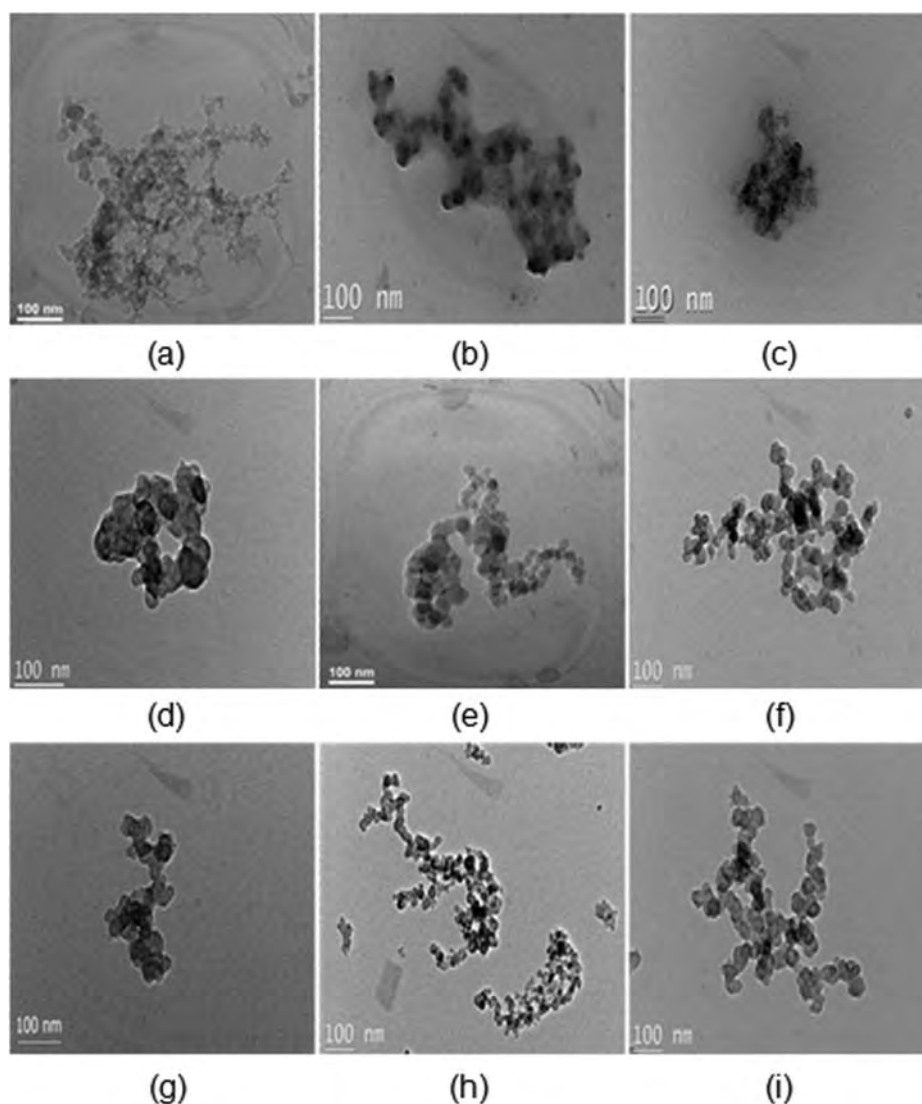
FIG. 3. TEM images of soot particles under high magnification from: (a) electric arc, (b) styrofoam burning, (c) plastic burning, (d) candle flame, (e) acetylene flame, (f) wood (white oak) burning in the flaming phase, (g) rice straw burning in the flaming phase, (h) diesel exhaust, and (i) kerosene flame.

carbon monoxide (CO) concentration and less oxygenated organic species, compared to the other parts of ponderosa pine wood. We also found that these spherical particles were refractory, as they were not sensitive to the increased electron beam intensity (i.e., high magnification), and that they contained inorganic species (e.g., S).

As shown in Figure 5, the acetylene flame, diesel exhaust, rice straw burning, and wood burning (white oak) soots all exhibited crystalline structures having ordered layers, while the plastic burning and wood burning (pine bark burning in the smoldering phase) soot showed an amorphous microstructure. The electric arc and styrofoam burning soot also showed an amorphous microstructure. The electric arc soot experienced a high cooling rate. If the cooling rate is fast, carbon clusters do not have enough energy and time to have an ordered crystalline structure,

leading to a disordered structure (Liu et al. 2004). For polymers, the monomers formed upon heating are created by a scission of the chain (Panagiotou and Levendis 1994). The polystyrene, a major component of the styrofoam container, had a branched structure with aromatics, while the polyethylene, a major component of the plastic bag, had a straight chain structure. Both fuels were harder to burn than other fuels and their flames were faint with a low sooting. They also had a significant amount of condensable species. It is possible that these conditions led to the amorphous structure of their primary particles.

The EDS data, included in Table 2, showed that C and O elements were found in all types of soot. Since elemental composition of particle free area was measured along with the EDS to account for background contribution, C, O, and Cu elements found in the EDS spectrum mostly come from particles. K and
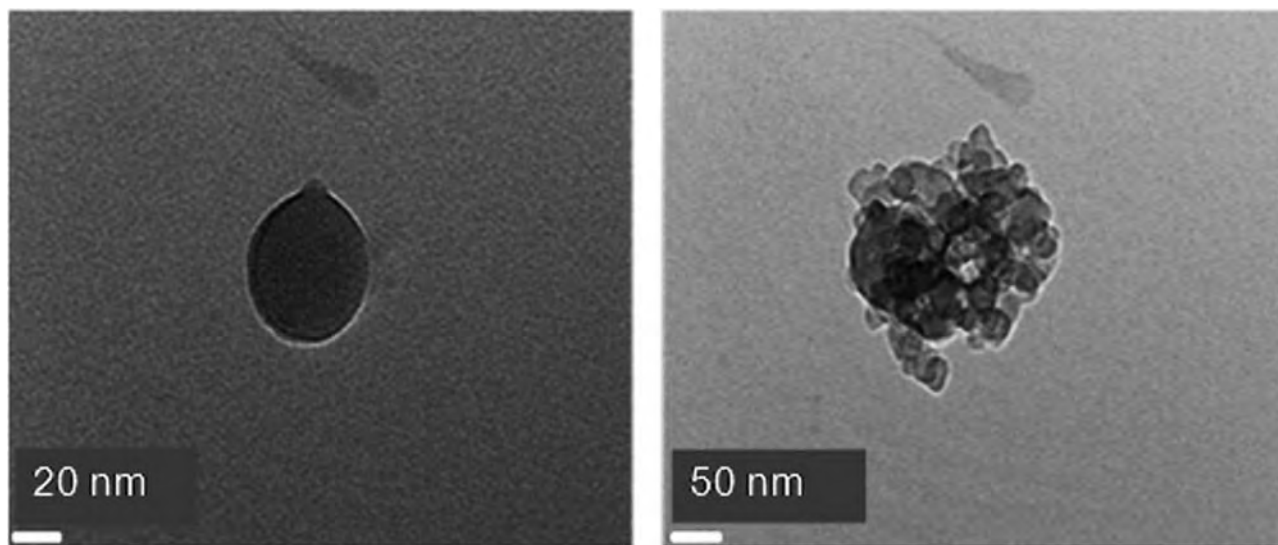
FIG. 4. TEM images of wood (pine bark) burning particles in the smoldering phase.

other inorganic species were detected in particles from wood (white oak and pine bark) burning and rice straw burning, suggesting that K could be used as a marker for fresh soot particles from biomass burning. The presence of K and other inorganic species such as Ca, Mg, and S makes the soot from vegetative burning more polar, hygroscopic, and probably more prone to aging. A bulk analysis of the soot from wood smoke showed a substantial fraction of inorganic salt, possibly enhancing their water solubility and hygroscopicity (Mavrocordatos et al. 2002).

Morphological and Elemental Classification of Atmospheric Ultrafine Particles

The properties of mobility-classified ultrafine particles sampled at the urban Gwangju, industrial Yeosu, and coastal Taean sites in Korea were investigated. Because of the diversity of atmospheric particles, we limited our attention to the ultrafine mode particles when an increase of ultrafine particle number concentration was observed, which was classified into photochemical and combustion events by Park et al. (2008). The number concentration of ultrafine particles was continuously monitored by the SMPS.

Our classification of atmospheric ultrafine particles is based on their morphology, elemental composition, and beam sensitivity. The agglomerates were classified as either "fresh agglomerates" or "aged agglomerates." The "fresh agglomerate" contained a major element of C along with a few minor elements and distinct primary particles, similar to the agglomerates reported in Table 2 and Figure 3, while the "aged agglomerate" contained multi elements and a visible coating or were coagulated with other types of particle. Since it is difficult to identify source of agglomerated soot particles in the ambient air, the atmospheric soot particles were roughly classified into "fresh" and "aged"

agglomerates. The classification of laboratory-generated soot particles, however, provides useful information on the type of soot particles, which may be observed in the other atmospheric or indoor condition.

Figure 6a shows a fresh agglomerate with no visible coating and a major element of C in its EDS spectrum. Figure 6b shows an aged agglomerate which was included in the sphere, having multi elements (e.g., S, Si, C). This particle type is similar to those found by Okada et al. (2003). When the electron beam in the TEM was intensified to magnify particle, the spherical species decomposed, suggesting that they are volatile. Figure 6c illustrates an aged agglomerate coagulated with spherical particles, resulting in the existence of multi elements such as C, O, Si, S, K, and Fe. These aged agglomerates may have undergone atmospheric processing (i.e., condensation and coagulation), leading to their more compact structure with additional chemical species (Zhang et al. 2008). The restructuring may depend on the origin of the soot. For instance, the soot agglomerates from the electric arc may collapse into more compact agglomerates when they are exposed to high relative humidity, but the diesel-exhaust particles may exhibit only minimal restructuring due to the presence of a hydrophobic organic coating such as lubricating oil, PAHs, and unburned hydrocarbons (Xue et al. 2009). In addition, we classified the atmospheric ultrafine particles as either sulfate mixtures (spherical), metallic oxides (spherical and polygonal), C-rich refractory (spherical), C-rich non-refractory (spherical), Si-rich (spherical), Na-rich (porous), or P-containing (non-spherical) particles, as summarized in Table 3. In case of sulfate mixtures they are spherical and usually contained S, coexisting with other elements. The classification of C-rich refractory (beam-resistant) and C-rich non-refractory (beam-sensitive) particles was determined by their response to the intensified electron beam in the TEM. The C-rich refractory
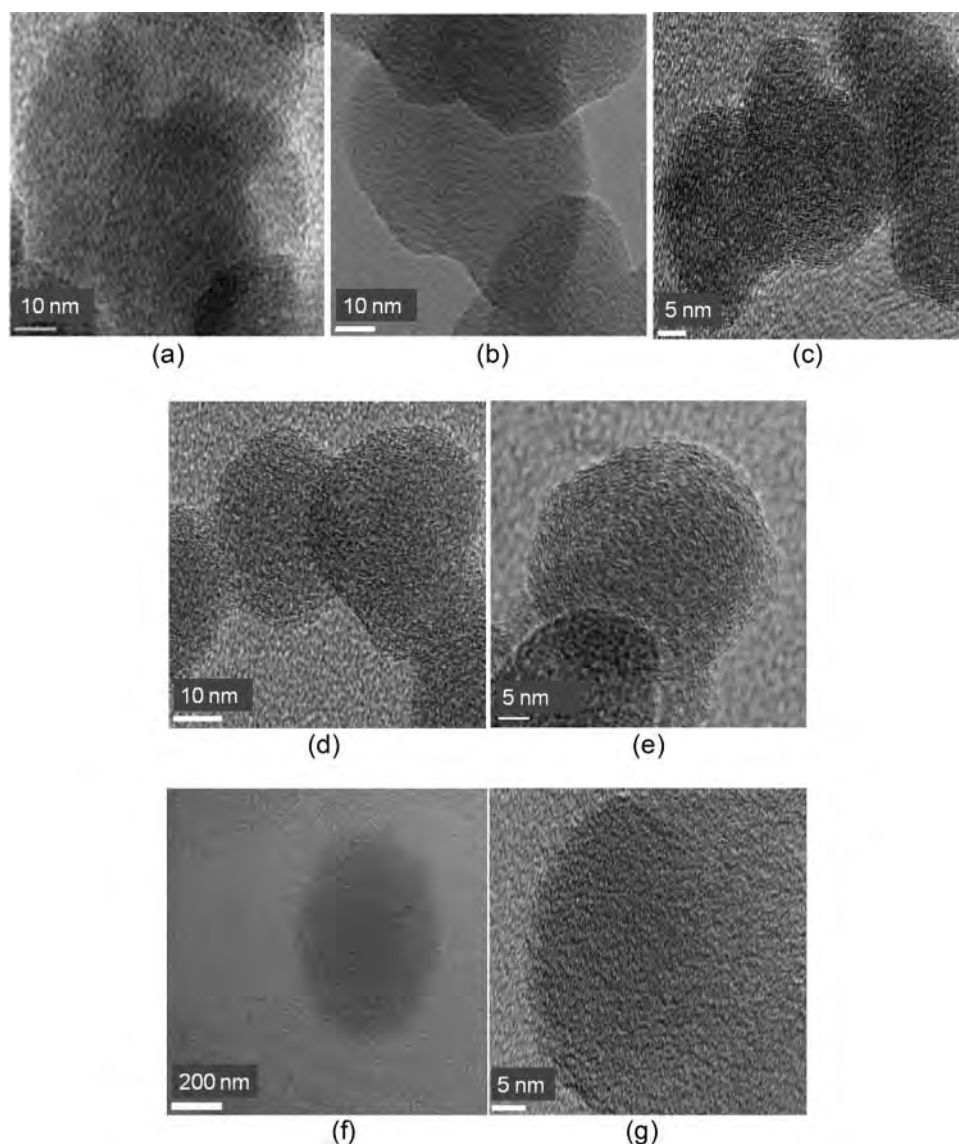
FIG. 5. Microstructure of soot or carbonaceous particles from: (a) acetylene flame, (b) rice straw burning in the flaming phase, (c) diesel exhaust, (d) white oak burning in the flaming phase, (e) kerosene flame, (f) pine bark burning in the smoldering phase, and (g) plastic burning.

particles were not agglomerated and had a major element of C, and exhibited no visible morphological change under the strong electron beam intensity in the TEM.

Figure 7a shows a TEM image of a sulfate mixture particle. When the electron beam in the TEM was intensified, a hollow area was frequently observed, indicating the presence of volatilized materials (Okada and Heintzenberg 2003). This type of spherical particle was particularly observed in the photochemical event (Park et al. 2008). The corresponding EDS spectrum showed a minor S, suggesting that sulfates evaporated under strong electron beam and high vacuum conditions in the TEM. Figures 7b and c show Cu-rich and Zn-rich metallic oxide (polygonal), respectively. The metallic oxide particles, often observed in urban and industrial sites, are opaque and often coated.

The Si-rich particle is spherical and sometimes contains minor Al, possibly originating from fly ash in a polluted atmosphere (Li et al. 2003; Niemi et al. 2006). The Na-rich particle contains Na, S, and K. The Na-S-K-O and porous morphology might be resulted from burning of biomass residuals or other waste material (Niemi et al. 2006). The P-containing particle usually has an abundant C with a minor P and may have a biological origin. Although microstructure of atmospheric particles was not examined in details, all of particles shown in Figures 6, 7, and 8 seem to be amorphous except for some fresh agglomerates.

Regardless of above morphological and elemental classification, two types of particles, refractory and non-refractory, can be identified based on their stability under high beam intensity in the TEM. The non-refractory particles are volatilized in
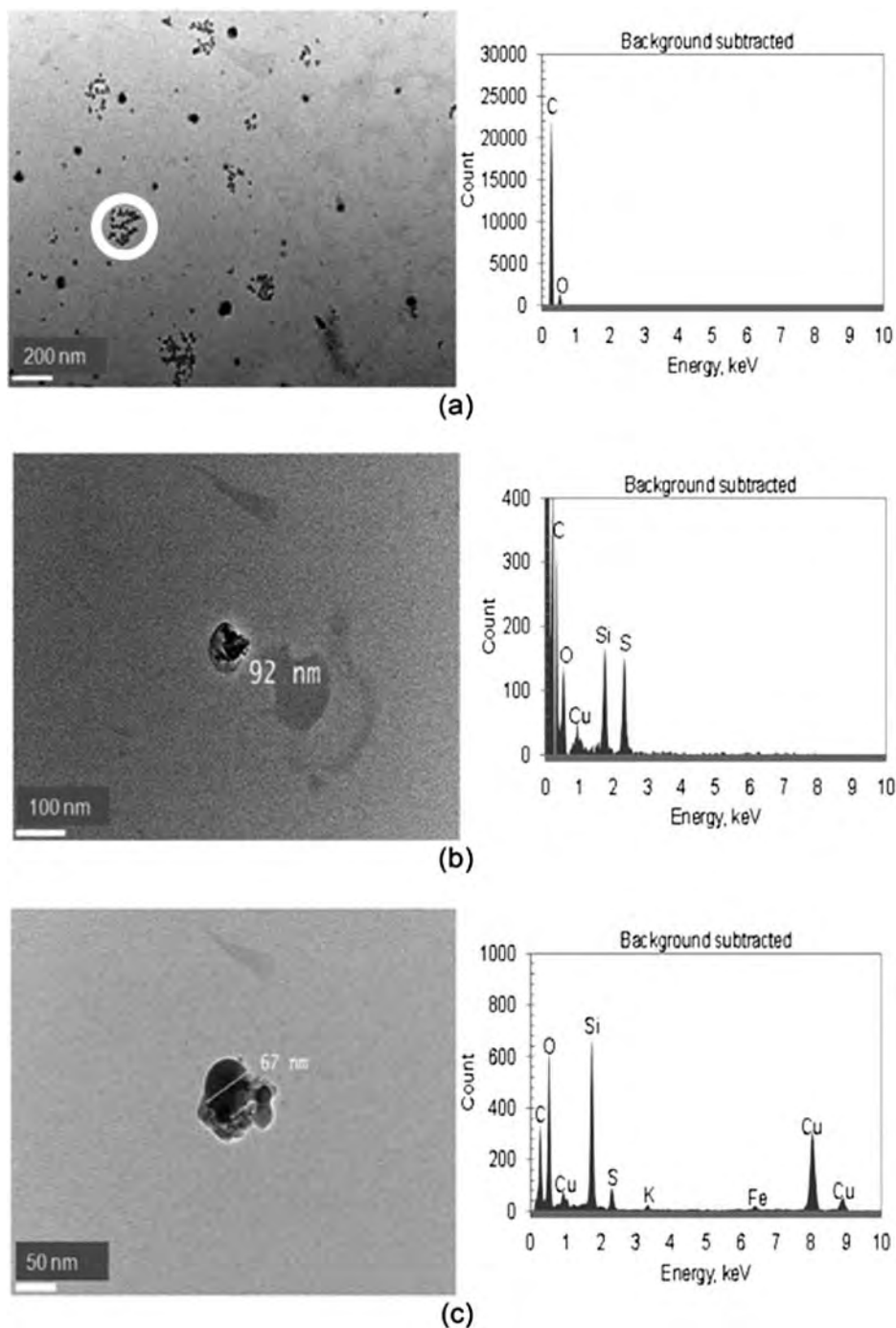
FIG. 6. TEM and EDS data of agglomerate particles sampled in the ambient atmosphere for: (a) fresh agglomerate, (b) aged agglomerate (coated), and (c) aged agglomerate (coagulated).

the TEM, leaving a residue, which is similar to the response of the laboratory-generated $(NH_4)_2SO_4$ particles, as shown in Figure 2. The non-refractory particles were the sulfate mixture and C-rich non-refractory particles. The particles classified as metallic oxides, C-rich refractory, Si-rich, and Na-rich, were refractory, comparable to the laboratory-generated PSL and NaCl particles, shown in Figure 2.

Comparison of Atmospheric Ultrafine Particles Among Different Sites

The number of each type of atmospheric ultrafine particles classified above was determined among the three different sites during ultrafine particle formation events. Note that particles more volatile than $(NH_4)_2SO_4$ were not included in the TEM analysis. Results for the laboratory-generated $(NH_4)_2SO_4$

TABLE 3
Summary of morphological and elemental properties of mobility-classified ultrafine atmospheric particles

| Particle type	Morphological description	Major elements	Minor elements	Mobility size (nm)	Number of particles at Gwangju	Number of particles at Yeosu	Number of particles at Taean
Fresh agglomerate	Distinct primary particles without heavy coating	C	O, Si, Cu	20, 25, 30, 35, 50, 70, 80, 90	46	4	3
Aged agglomerate	Coated, coagulated, or mixed with other chemical elements	C, O, S, Cu, Ca, Mg	Si, Ti, Fe, Na, K, Cl, Al	25, 30, 35, 40, 50, 70, 80, 90, 100, 160	49	7	0
Sulfate mixture	Spherical morphology and presence of beam-damaged portion at high magnification	S, C, O	Ca, Mg, K, Cu, Na, Al	20, 25, 30, 35, 50, 70, 80, 160	78	5	3
Metallic oxides	Opaque spherical or polygonal	C, O, Cu, Al, Si, Ca, Fe, Cr, Zn	Ti, K, Mg, Cl	20, 25, 30, 35, 40, 50, 70, 80, 160	185	29	11
C-rich refractory	Not agglomerated and beam-resistant at high magnification	C	O, Si, Cu	20, 25, 30, 35, 50, 80, 130, 160	278	60	7
C-rich non-refractory	Not agglomerated and beam-sensitive at high magnification	C	O, Cu, Si	20, 25, 30, 35, 40, 50, 70, 80, 100, 130	146	25	8
Si-rich	Spherical and beam-resistant	Si, C, O, Cu	Al, Ca, Mg, K, Na	30, 35, 40, 50, 70, 80, 160	5	24	3
Na-rich	Porous and rounded edges	Na, C, K, Cl, Cu	O, S	35, 40, 50, 80	5	18	0
P-containing	Elongated or aggregated	C, O, P	Si, Cu, Ca, Zn, Fe, Cl	35, 70, 80, 100	21	1	1
	Total				813	173	36
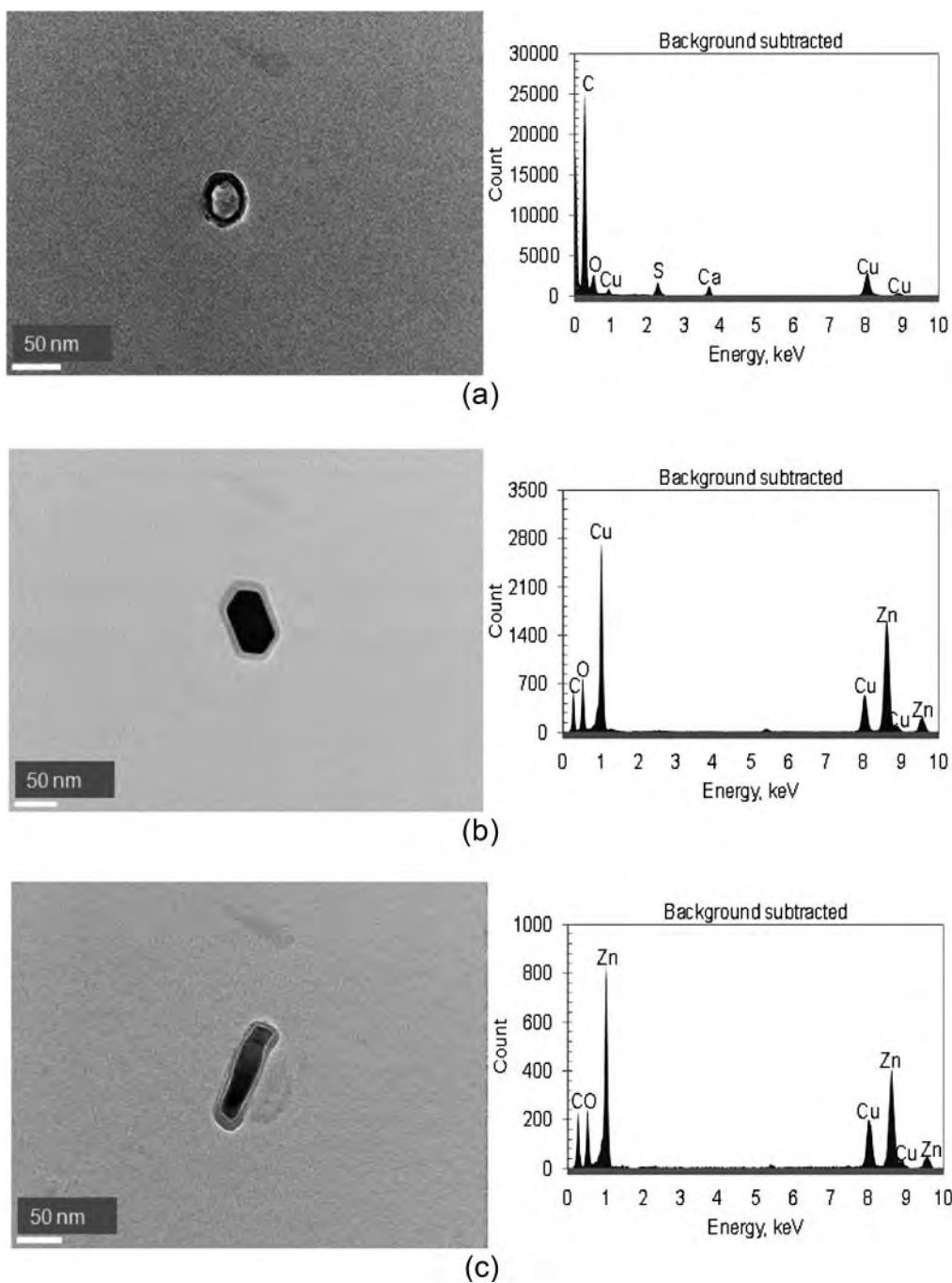
FIG. 7. TEM-EDS data of: (a) sulfate mixture, (b) Cu-rich metallic oxide (polygonal), and (c) Zn-rich metallic oxide (polygonal).

particles (<100 nm) showed that they did not evaporate under low electron beam intensity and partially evaporated under high electron beam intensity. The C-rich non-refractory particles defined here showed a similar behavior to the $(NH_4)_2SO_4$ particles. Table 3 compares the number of each type of ultrafine particles in the three sampling sites. We observed relatively higher fraction of agglomerates (both fresh and aged) at the urban Gwangju site and the appearance of fresh agglomerates was consistent with

the combustion event at this site (Park et al. 2008). In this combustion event, caused primarily by traffic and residential heating, the peak mode size of ultrafine particles was 70–100 nm, while a lower mode size (10–50 nm) was observed in the photochemical event. In the photochemical event at the urban Gwangju site, C-rich non-refractory and sulfate mixtures were often observed. The C-rich refractory, metallic oxide particles, and Si-rich particles are abundant at the industrial Yeosu site.
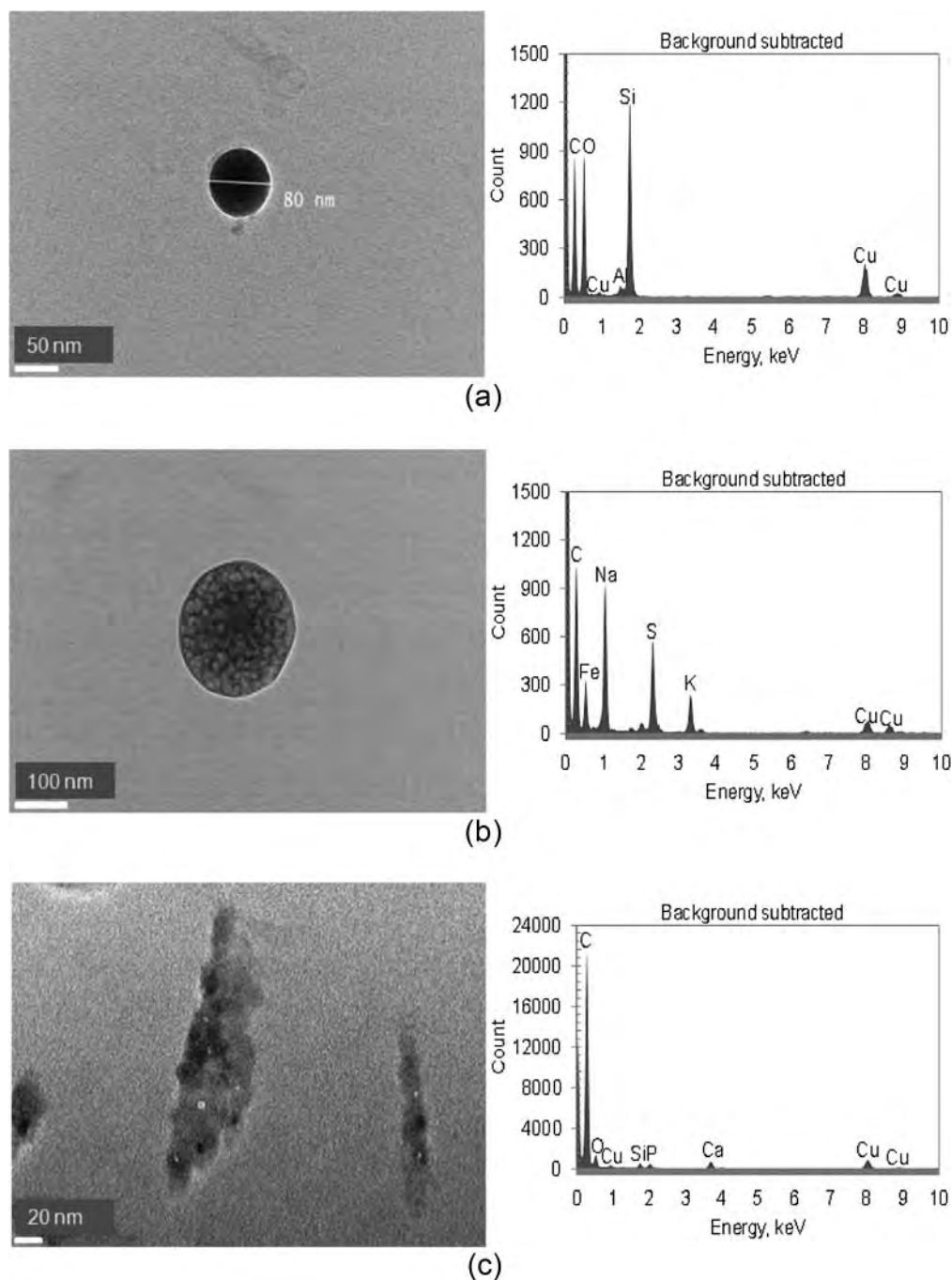
FIG. 8. TEM-EDS of: (a) Si-rich particle, (b) Na-rich particle, and (c) P-containing particle.

The metallic oxides can be contributed by the steel industries at the Yeosu site. The Si-rich particles can originate from petrochemical industries where zeolites or silicates are abundantly used as catalysts (Mravec et al. 2005). At the background Taean site the ultrafine particles were not as diverse as those from urban or industrial site, and few agglomerates were observed due to the absence of anthropogenic combustion sources in this area.

CONCLUSIONS

This study was conducted to examine morphological and elemental properties of fresh soot particles produced from a variety of fuels and processes, and to classify atmospheric ultrafine particles sampled at three ambient sampling sites (urban Gwangju, industrial Yeosu, and coastal background Taean) during ultrafine particle formation event. A laboratory test showed a significant morphological change for non-refractory particles

like $(NH_4)_2SO_4$ (100 nm) between low and high magnification, while refractory NaCl (100 nm) and PSL (84 nm) showed no difference, suggesting that morphological properties of more volatile particles than $(NH_4)_2SO_4$ cannot be accurately determined by the TEM method. Distinct differences in morphological properties were observed among the different types of fresh soot particles. The diesel soot particles had the lowest fractal dimension (1.69), suggesting that they are the most irregular among the fresh soot particles tested here. An examination of the microstructures of the primary particles revealed that plastic burning, styrofoam burning, electric arc, pine bark burning (in the smoldering phase), and rice straw burning (in the smoldering phase) soot had amorphous microstructures, while others exhibited crystalline structures having ordered layers. The soot produced from burning wood and rice straw showed K in its EDS spectrum, potential marker for biomass burning emissions. A comparison between wood combustion in the flaming phase (white oak) and the smoldering phase (pine bark) revealed that the flaming phase produced fractal-like particles, while the smoldering phase produced a significant number of tar ball-like particles (spherical). The atmospheric ultrafine particles were classified as being fresh agglomerate, aged agglomerate, sulfate mixture (spherical), metallic oxides (spherical and polygonal), C-rich refractory, C-rich non-refractory (spherical), Si-rich (spherical), Na-rich (porous), or P-containing particles (nonspherical). The fresh and aged agglomerates were found to be abundant at the urban Gwangju site, and C-rich non-refractory and sulfate mixtures were often observed in the photochemical event at this site. The Si-rich and C-rich refractory particles were abundant at the industrial Yeosu site. The coastal Taean site did not have as diverse particle types as compared to other sites and had least agglomerates due to limited anthropogenic combustion sources.

REFERENCES

Barone, T. L., and Zhu, Y. (2008). The Morphology of Ultrafine Particles on and Near Major Freeways. *Atmos. Environ.* 42:6749–6758.

Bond, T. C., and Bergstrom, R. W. (2006). Light Absorption by Carbonaceous Particles: An Investigative Review. *Aerosol Sci. Technol.* 40:27–67.

Dobbins, R. A. (2007). Hydrocarbon Nanoparticles Formed in Flames and Diesel Engines. *Aerosol Sci. Technol.* 41:485–496.

Friedlander, S. K. (2000). *Smoke, Dust, and Haze Fundamentals of Aerosol Dynamics*, 2nd *Edition*. Oxford University Press, New York, p. 372.

Grieshop, A. P., Logue, J. M., Donahue, N. M., and Robinson, A. L. (2009). Laboratory Investigation of Photochemical Oxidation of Organic Aerosol from Wood Fires 1: Measurement and Simulation of Organic Aerosol Evolution. *Atmos. Chem. Phys.* 9:1263–1277.

Hu, B., and Koylu, U. (2004). Size and Morphology of Soot Particulates Sampled from a Turbulent Nonpremixed Acetylene Flame. *Aerosol Sci. Technol.* 38:1009–1018.

Jung, H., Kittelson, D. B., and Zachariah, M. R. (2004). Kinetics and Visualization of Soot Oxidation using Transmission Electron Microscopy. *Combust. Flame.* 136:445–456.

Katrinak, K. A., Rez, P., and Buseck, P. R. (1992). Structural Variations in Individual Carbonaceous Particles from an Urban Aerosol. *Environ. Sci. Technol.* 26:1967–1976.

Katrinak, K. A., Rez, P., Perkes, P. R., and Buseck, P. R. (1993). Fractal Geometry of Carbonaceous Aggregates from an Urban Aerosol. *Environ. Sci. Technol.* 27:539–547.

Kim, W., Sorensen, C. M., Fry, D., and Chakrabarti, A. (2006). Soot aggregates, Superaggregates, and Gel-Like Networks in Laminar Diffusion Flames. *J. Aerosol Sci.* 37:386–401.

Kocbach, A., Li, Y., Yttri, K. E., Cassee, F. R., Schwarze, P. E., and Namork, E. (2006). Physicochemical Characterisation of Combustion Particles from Vehicle Exhaust and Residential Wood Smoke. *Part. Fibre Toxicol.* 3:1–10.

Li, J., Anderson, J. R., and Buseck, P. R. (2003). TEM Study of Aerosol Particles from Clean and Polluted Marine Boundary Layers over the North Atlantic. *J. Geophys. Res.* 108:8-1-8-14.

Liu, Y., Xiaolong, S., Tingkai, Z., Jiewu, Z., Hirscher, M., and Philipp, F. (2004). Amorphous Carbon Nanotubes Produced by a Temperature Controlled DC Arc Discharge. *Carbon.* 42:1852–1855.

Mavrocordatos, D., Kaegi, R., and Schmatloch, V. (2002). Fractal Analysis of Wood Combustion Aggregates by Contact Mode Atomic Force Microscopy. *Atmos. Environ.* 36:5653–5660.

Maynard, A. D. (2000). Overview of Methods for Analysing Single Ultrafine Particles. *Phil. Trans. R. Soc. Lond. A.* 358:2593–2610.

Mckenzie, L. M., Hao, W. M., Richards, G. N., and Ward, D. E. (1995). Measurement and Modeling of Air Toxins from Smoldering Combustion of Biomass. *Environ. Sci. Technol.* 29:2047–2054.

Mravec, D., Hudec, J., and Janotka, I. (2005). Some Possibilities of Catalytic and Noncatalytic Utilization of Zeolites. *Chem. Pap.* 59:62–69.

Niemi, J. V., Saarikoski, S., Tervahattu, H., Mäkelä, T., Hillamo, R., Vehkamäki, H., Sogacheva, L., and Kulmala, M. (2006). Changes in Background Aerosol Composition in Finland During Polluted and Clean Periods Studied by TEM/EDX Individual Particle Analysis. *Atmos. Chem. Phys.* 6:5049–5066.

Oberdörster, G., Oberdörster, E., and Oberdörster, J. (2005). Nanotoxicology: An Emerging Discipline Evolving from Studies of Ultrafine Particles. *Environ. Health Pers.* 113:823–839.

Oberdörster, G. (2001). Pulmonary Effects of Inhaled Ultrafine Particles. *Occup. Environ. Health*.74:1–8.

Oberdörster, G. (2000). Toxicology of Ultrafine Particles: In Vivo Studies. *Phil. Trans. R. Soc. A.* 358:2719–2740.

Oh, C., and Sorensen C. M. (1997). The Effect of Overlap between Monomers on the Determination of Fractal Cluster Morphology. *J. Colloid Interface Sci.* 193:17–25.

Okada, K., and Heintzenberg, J. (2003). Size Distribution, State of Mixture, and Morphology of Urban Aerosol Particles at Given Electrical Mobilities. *J. Aerosol Sci.* 34:1539–1553.

Panagiotou, T., and Levendis, Y. (1994). A Study on the Combustion Characteristics of PVC, Poly(styrene), Poly(ethylene), and Poly(propylene) Particles under High Heating Rates. *Combust. Flame.* 99:53–74.

Park, K., Cao, F., Kittelson, D. B., and McMurry, P. H. (2003). Relationship Between Particle Mass and Mobility for Diesel Exhaust Particles. *Environ. Sci. Technol.* 37:577–583.

Park, K., Kittelson, D. B., and McMurry, P. H. (2004). Structural Properties of Diesel Exhaust Particles Measured by Transmission Electron Microscopy (TEM): Relationships to Particle Mass and Mobility. *Aerosol Sci. Technol.* 38:881–889.

Park, K., Park, J., Kwak, J., Cho, G., and Kim, J. (2008). Seasonal and Diurnal Variations of Ultrafine Particle Concentration in Urban Gwangju, Korea: Observation of Ultrafine Particle Events. *Atmos. Environ.* 42:788–799.

Peters, A., Wichmann, H. E., Tuch, T., Heinrich, J., and Heyder, J. (1997). Respiratory Effects are Associated with the Number of Ultrafine Particles. *Am. J. Respir. Crit. Care Med.* 155:1376–1383.

Posfai, M., Simonics, R., Li, J., Hobbs, P. V., and Buseck, P. R. (2003). Individual Aerosol Particles from Biomass Burning in Southern Africa: 1. Compositions and Size Distributions of Carbonaceous Particles. *J. Geophys. Res.* 108:19-1-19-13.

Pugmire, R. J., Solum, M. S., Jiang Y. J., Sarofim A. F., Veranth, J., Schobert H. H., and Pappano, P. J. (2002). The Study of Soot Formation by Solid State NMR Spectroscopy . *Fuel Chem. Div. Preprints.* 47:733–735.

Stearns, R. C., Paulauskis, J. D., and Godleski, J. J. (2001). Endocytocis of Ultrafine Particles by A549 Cells. *Am. J. Respir. Cell. Mol. Biol.* 24:108–115.

Szidat, S., Prevot A. S. H., Sandradewi, J., Alfarra, M. R., Synal, H.-A., Wacker, L., and Baltensperger, U. (2007). Dominant Impact of Residential Wood Burning on Particulate Matter in Alpine Valleys during Winter. *Geophys. Res. Lett.* 34: L05820.

Wentzel, M., Gorzawski, H., Naumann, K.-H., Saathoff, H., and Weinbruch, S. (2003). Transmission Electron Microscopical and Aerosol Dynamical Characterization of Soot Aerosols. *J. Aerosol Sci.* 34:1347–1370.

Xiong, C., and Friedlander, S. K. (2001). Morphological Properties of Atmospheric Aerosol Aggregates. *Proc. Natl. Acad. Sci*. 98:11851–11856.

Xue, H., Khalizov, A. F., Wang, L., Zheng, J., and Zhang, R. (2009). Effects of Coating of Dicarboxylic Acids on the Mass-Mobility Relationship of Soot Particles. *Environ. Sci. Technol*. 43:2787–2792.

Zhang, R., Khalizov, A. F., Pagels, J., Zhang, D., Xue, H., and McMurry, P. H. (2008). Variability in Morphology, Hygroscopicity, and Optical Properties of Soot Aerosols During Atmospheric Processing. *Proc. Natl. Acad. Sci.* 105:10291–10296.